Korean J. Chem. Eng., 40(1), 215-222 (2023)
DOI: 10.1007/s11814-022-1263-4

pISSN: 0256-1115
eISSN: 1975-7220

Removal of fluoroquinolone antibiotics by adsorption of dopamine-modified biochar aerogel

Hongjuan Bai†, Qiaofei Zhang, Xuan Zhou, Junhang Chen†, Zihan Chen, Zhuangzhuang Liu, Jun Yan, and Jing Wang

School of Chemistry and Chemical Engineering, Henan University of Technology, Zhengzhou 450001, P. R. China
(*Received 21 April 2022 • Revised 7 June 2022 • Accepted 17 August 2022*)

Abstract−As emerging contaminants used for treating various tract infections, fluoroquinolones (such as enoxacin, ofloxacin, etc.) enter water bodies via point-source discharges of wastewater treatment plants and many of them raise environmental and health concerns. Herein, a novel adsorbent, derived from a useful renewable low-cost grapefruit peel, was prepared to investigate the adsorption behavior of fluoroquinolone antibiotics (enoxacin and ofloxacin). The obtained adsorbent was characterized by scanning electron microscopy (SEM), Fourier transform infrared (FTIR), X-ray diffraction (XRD) and thermo-gravimetric analysis and differential scanning calorimetry (TG-DSC). Further, the equilibrium sorption of the adsorption process was analyzed with isotherm models and kinetic models. Under optimal adsorption conditions, equilibrium data conformed to the Elovich model, and the kinetics of adsorption was fitted well with Redlich-Peterson model. Combined with thermodynamic analysis, electrostatic interaction, hydrogen bond, π-π stacking interaction were the possible adsorption mechanisms for both fluoroquinolone antibiotics onto the novel adsorbent. This work explored a promising adsorbent for the elimination of fluoroquinolone antibiotics in environmental remediation.

Keywords: Adsorption, Biomass, Fluoroquinolone Antibiotics, Wastewater Treatment

INTRODUCTION

Fluoroquinolone antibiotics are widely used for improving human health and as special drugs for livestock farms [1]. Since most antibiotics are malabsorbed and not fully metabolized in humans and animals, most antibiotics used (30-90%) are released into the environment through human and animal urine and feces [2]. Enoxacin (ENO), the most representative fluoroquinolone antibiotic, is frequently used in the treatment of systemic bacterial infections, lepromatous leprosy. Ofloxacin (OFLX), a critical member of fluoroquinolone antibiotics, is often utilized to treat wound infections, respiratory tract infections. In fact, even at low concentrations, the existence of antibiotics in the environment will lead to the proliferation of drug-resistant bacteria and imperil ecological security [3]. With the increasing impact of these antibiotics on the environment, the treatment of these pollutants has become more and more important.

Among the methods (for example, coagulation, oxidation, reverse osmosis, adsorption) for removal of fluoroquinolone antibiotics from wastewater, adsorption has been widely used in environmental remediation because of its environmental-friendliness, low cost and low requirements for reaction conditions [4]. A variety of adsorbents had been developed for fluoroquinolone antibiotics removal, such as gelatum, metal-organic frameworks, functionalized magnetic nanoparticles, zeolite, and biochar [5]. After Marris and Lehmann proposed the carbon sequestration and soil improvement of biochar, the application of biochar began to attract extensive attention [1,6,7]. Carbon aerogel (a branch of aerogels) is a special porous material, which is usually pyrolyzed in an inert gas atmosphere by pyrolysis of organic aerogels as precursors. It has a porous surface, large specific surface area, low density and good expansibility. And it has an open three-dimensional network structure, which is conducive to the adsorption of pollutants [8]. Biomass resources are widely distributed, with low cost, abundant carbon sources and remarkable benefits. The preparation of environment-friendly porous carbon aerogels by using abundant biomass materials is an economic and sustainable way of development [9]. In addition, these excellent properties, combined with its easily modified surface properties, these materials are suitable for a series of environmental protection applications [10,11]. Geng et al. nitrated walnut shell biochar to obtain an efficient sulfonamide adsorbent for adsorbing sulfadiazine, sulfamethazine and sulfa chloropyridine from aqueous solution [12]. Grapefruit is widely grown in tropical and subtropical regions around the world, and there is a large amount of grapefruit peel waste [13]. Huang et al. modified grapefruit peel biochar with 3-amino-5-mercapto-1,2,4-triazole to improve the capacity of Pb (II) removal from wastewater [14]. Dopamine has self-polymerization (PDA) and can form a hydrophilic surface attached PDA coating on biomass carbon materials, which can make toxic pollutants adequately and tightly contact with adsorbents in water [15]. However, to our knowledge, no data were found in the published literature, focusing on the grapefruit peel biochar aerogels modified by the dopamine as an adsorbent to remove enoxacin (ENO) and ofloxacin (OFLX) from aqueous solutions.

In this work, biochar aerogel derived from grapefruit peel was

†To whom correspondence should be addressed.
E-mail: hongjuan.bai@haut.edu.cn, chenjunhang@haut.edu.cn

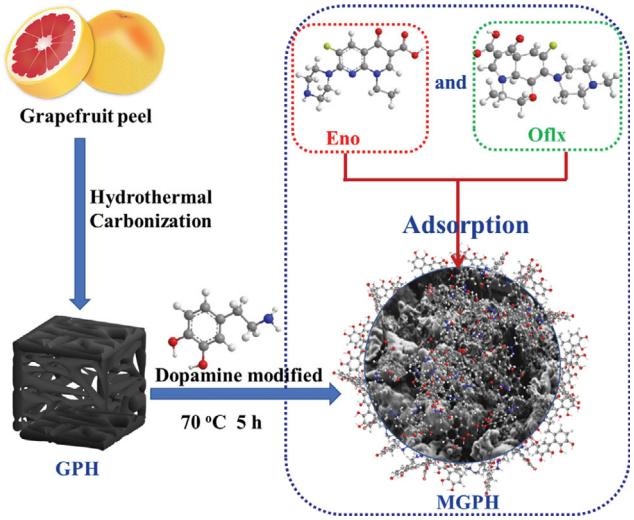

Scheme 1. Schematic preparation processes of MGPH for ENO and OFLX adsorption.

prepared, and then the grapefruit peel biochar aerogel was modified by dopamine (MGPH) to remove the ENO and OFLX from aqueous solutions. The simple fabrication process is illustrated in Scheme 1. The physicochemical properties of MGPH were investigated by various characterization methods. The effect of pH on adsorption performance was evaluated by static adsorption experiment. Adsorption isotherms, kinetics and thermodynamics were also investigated to understand the adsorption mechanisms of ENO and OFLX onto MGPH.

MATERIALS AND METHODS

1. Reagents and Solutions

Grapefruit was produced in Fujian, and all the solutions were prepared with ultrapure water (EASY Pure II water system, Iowa USA). Other experimental reagents used in this study are shown in Table S1. The structure and physicochemical properties of ENO and OFLX are shown in Table 1.

2. Adsorbent Preparation and Modification used in this Study

First, cleaned fresh grapefruit peel was cut into 1 cm^3 blocks. Then it was put into an oven at 30 °C to dry to constant weight, put into a hydrothermal reactor, react at 180 °C for 12 h, and cool naturally to room temperature. The obtained solid was immersed in a 1 : 1 solution of alcohol and deionized water for 12 h, and then the solid material was soaked with deionized water until the cleaning solution was colorless and transparent. The solid was placed in the refrigerator at −18 °C for 12 h, then dried at −60 °C for 50 h until the solid material changed from black to brown, and the hydrothermal carbonization of grapefruit peel aerogel (GPH) was obtained. 0.5 g aerogel and 0.5 g dopamine were dispersed in 250 mL pH 8.5 Tris solution, stirred 5 h at constant temperature at 70 °C and filtered by vacuum, then dried in a 50 °C vacuum drying oven for 8 h, marked as MGPH.

3. Characterizations

The surface morphology was obtained by SEM (Hitachi SU8100, Japan). Fourier Transform infrared (FTIR) spectra were recorded from 400 to 4,000 cm^{-1} on a spectrometer (Bruker Vertex 70, German). The surface element composition of MGPH was analyzed by X-ray diffraction (Bruker D8 Advance, German), where 2θ ranged from 10 to 80°. Thermal stability and thermal decomposition were studied by thermogravimetric analysis (TGA 550, USA), about 10 mg of MGPH was heated to 800 °C in oxidant atmosphere at 10 min^{-1} temperature rate. The specific surface area and pore size distribution of adsorbents were measured with A high-speed automated surface area and pore size analyzer (Quantachrome Autosorb IQ3, USA), The specific surface area, pore size, and pore volume were then calculated according to the Brunauer-Emmett-Teller (BET) method and BJH method from the physical adsorption that occurred on the surface of the samples at 77 K. X-ray photoelectron spectroscopy (XPS) was performed using a Thermo ESCALAB 250XI X-ray photoelectron system (Thermo Electron Corporation, USA). The point of zero charge of MGPH was measured to determine the net electrical neutrality of the adsorbent surface.

4. Adsorption Experiments

4-1. Effect of Solution pH on ENO and OFLX Removal

Experiments were carried out at different pH to study the effect of pH on adsorption. 0.01 g of MGPH was put into 50 mL conical flask containing 10 mL ENO or OFLX solution respectively, the pH of which ranged from 2 to 10. The flasks were then rotated at 150 rpm in a shaking box for two hours, which was sufficient to

Table 1. Physicochemical properties of enoxacin (ENO) and ofloxacin (OFLX)

Antibiotic	CAS	Molecular structure	Molecular formula	Molecular weight	pK_a	Suppliers
Enoxacin	74011-58-8	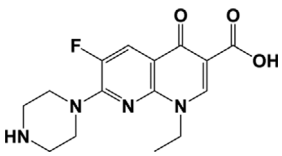	$C_{15}H_{17}FN_4O_3$	320.32	pK_{a1}=5.31 pK_{a2}=8.68	Rhawn®
Ofloxacin	82419-36-1	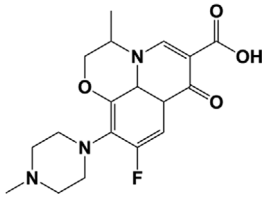	$C_{18}H_{20}FN_3O_4$	361.37	pK_{a1}=6.01 pK_{a2}=8.25	Rhawn®

reach adsorption equilibrium. ENO was measured at λ_{max} 266 nm and OFLX was determined at λ_{max} 288 nm respectively, by a UV-VIS spectrophotometer (PUXI TU1810).

4-2. Adsorption Thermodynamic Experiments

Isothermal adsorption experiments were performed at 293 K, 303 K and 313 K. 0.01 g of MGPH was put into 50 mL conical flask containing 10 mL ENO or OFLX solution with a concentration of 10-100 mg L^{-1}. The flasks were then agitated in a shaker at 150 rpm for 2 h. At three temperatures, three parallel sets of samples were prepared at each initial concentration. The experimental results obtained from the adsorption experiment were fitted by Langmuir, Freundlich, Redlich-Peterson and Dubinin-Radushkevich models, respectively. The expressions of these models are as follows [16-18]:

$$\text{Langmuir model: } q_e = \frac{q_{max} K_L C_e}{1 + K_L C_e} \quad (1)$$

$$\text{Freundlich model: } q_e = K_F C_e^{1/n} \quad (2)$$

$$\text{Redlich-Peterson model: } q_e = \frac{AC_e}{1 + BC_e^g} \quad (3)$$

$$\text{Dubinin-Radushkevich model: } q_e = q_m \exp\left[\frac{\left(RT\ln\left(1+\frac{1}{C_e}\right)\right)^2}{-2E^2}\right] \quad (4)$$

where C_e (mg L^{-1}) is the equilibrium dye concentration, q_e (mg g^{-1}) and q_{max} (mg g^{-1}) are the equilibrium and monolayer adsorption quantity of antibiotic. K_L (L mg^{-1}), K_F (mg^{1-n} L^n g^{-1}) and A (L g^{-1}) are the Langmuir, Freundlich and Redlich-Peterson constants, and 1/n is the indicator of adsorption intensity, E (kJ mol^{-1}) is adsorption energy, R (J mol^{-1} K^{-1}) is universal gas constant; T (K) is absolute temperature.

4-3. Adsorption Kinetics Experiments

The investigation of adsorption kinetics is of great importance as it facilitates the understanding of the adsorption mechanism and potential rate-controlling steps. The adsorption kinetics were investigated at initial concentrations of 30 mg L^{-1}, 50 mg L^{-1} and 80 mg L^{-1}, respectively. 0.01 g of MGPH was put into 50 mL conical flask containing 10 mL ENO or OFLX solution. Then oscillated in the vibrating screen at 150 rpm for 2, 5, 10, 15, 20, 30, 60, 90 and 120 min, respectively. Three groups of parallel samples with different oscillation time were prepared at three initial concentrations. The experimental results obtained from adsorption experiments were fitted with pseudo-first-order, pseudo-second-order, Elovich, double-constant rate and intra-particle diffusion (IPD) models, respectively. The expression of the models referred above are as follows [19,20]:

$$\text{Pseudo-first-order equation: } q_t = q_e(1 - e^{k_1 t}) \quad (5)$$

$$\text{Pseudo-second-order equation: } q_t = \frac{k_2 q_e^2 t}{1 + k_2 q_e t} \quad (6)$$

$$\text{Elovich equation: } q_t = \frac{1}{b}\ln(1 + abt) \quad (7)$$

$$\text{Double-constant rate equation: } q_t = at^{k_s} \quad (8)$$

$$\text{Intra-particle diffusion model: } q_t = k_t t^{0.5} + C \quad (9)$$

where q_e and q_t (mg g^{-1}) are the antibiotic adsorption quantity at equilibrium and at time t (min), respectively. k_1, k_2 and k_t (min^{-1}) are the adsorption rate constant of pseudo-first-order, pseudo-second-order (g mg^{-1} min^{-1}) and intra-particle diffusion (mg g^{-1} $min^{-1/2}$), respectively. a and B are constants, and C is the intercept of the intra-particle diffusion model.

4-4. Adsorption Thermodynamic Studies

The main parameters of adsorption thermodynamics are Gibbs free energy (ΔG, kJ mol^{-1}), enthalpy change (ΔH, kJ mol^{-1}), and entropy change (ΔS, kJ mol^{-1} K^{-1}). These thermodynamic parameters conform to the formulas [21]:

$$K_C = \frac{C_{ad,e}}{C_e} \quad (10)$$

$$\Delta G = -RT\ln K_C \quad (11)$$

$$\Delta G = \Delta H - T\Delta S \quad (12)$$

where K_C is the apparent equilibrium constant, $C_{ad,e}$ (mg g^{-1}) is the concentration of adsorbate on the adsorbent when the adsorption reaches equilibrium, C_e (mg g^{-1}) is when the adsorption reaches equilibrium, the concentration of adsorbate in the solution.

RESULTS AND DISCUSSION

1. Characterization of Adsorbent

The SEM image of GP shows that the surface of GP was smooth and there were many channels (Fig. 1(a)). GPH, after hydrothermal carbonization, formed a neat sheet structure, which increased the surface area of GPH (Fig. 1(b)). This may be because freeze-drying could reduce the collapse of three-dimensional porous structure, resulting in the formation of ultra-lightweight porous structure aerogels. Dopamine (DA) released protons to produce intermediate dihydroxyindole, and finally polydopamine was spontaneously synthesized between aerogels. Compared with the isolated GPH, MGPH was provided by polydopamine with a strong adhesion force, which interspersed in the aerogel film layer, resulting in a honeycomb three-dimensional porous structure (Fig. 1(c)), so that the modified aerogel specific surface area increased, which was conducive to the adsorption of fluoroquinolone antibiotics on its effective adsorption sites.

The BET specific surface area of MGPH and GP was analyzed by nitrogen adsorption-desorption isotherms (Fig. S1) were 8.32 and 0.094 m^2/g, respectively. The pore size distribution of MGPH had an average pore size of 12.48 nm and volume of 0.038 cm^3/g. This indicated that the adsorption capacity of the MGPH was strong when it was applied for pollutants adsorption.

The FT-IR spectra of the materials used in this work are shown in Fig. 1(d). A band at 3,310-3,350 cm^{-1} indicates the stretching vibration of O-H and N-H groups from the absorbed water. It widened and weakened in MGPH, which was connected with dopamine modification [22]. As for GP, the characteristic peak around 2,918 cm^{-1} represents methylene -CH_2 stretching vibration [1]. The characteristic peak around 1,613 cm^{-1} and 1,739 cm^{-1} represents C=O stretching of -COOH [23], and the peak around 1,015 cm^{-1} represents C-O stretching vibration. It and the C-O-C stretching vibration of ether bond at 1,236 cm^{-1} suggest that GP contained total

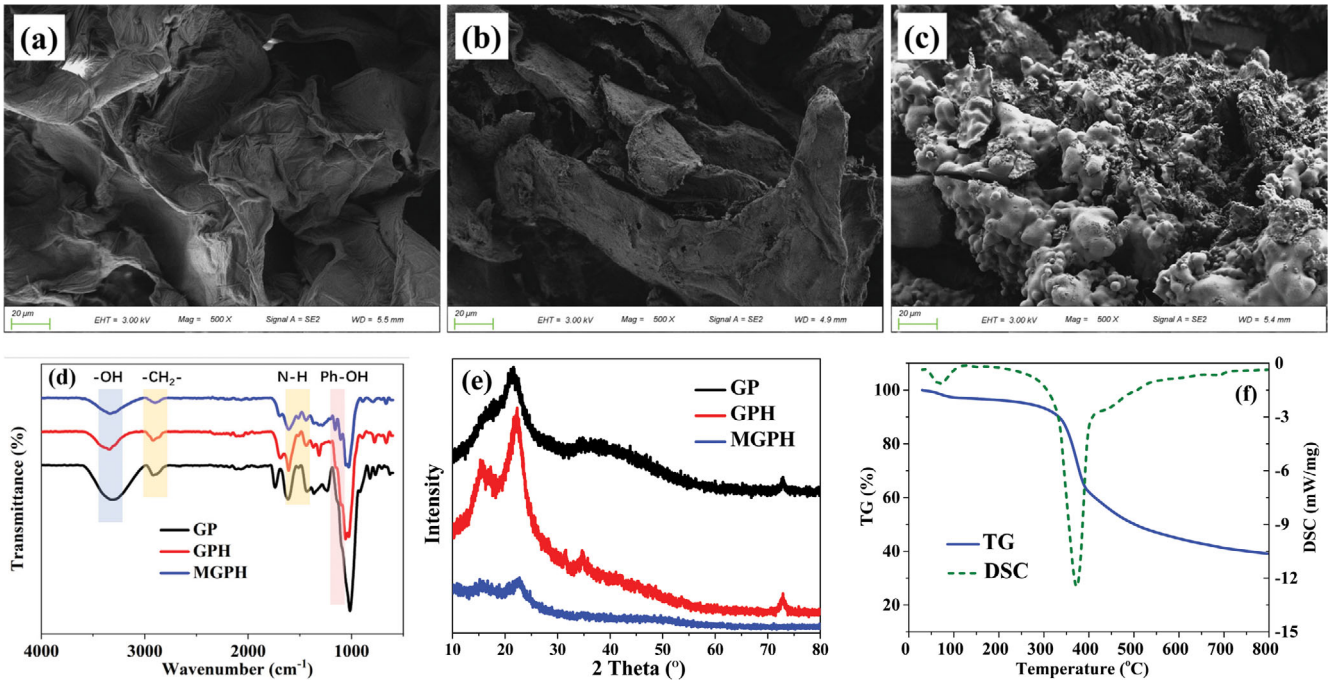

Fig. 1. Characterization: the SEM of GP (a), GPH (b) and MGPH (c); the FTIR (d); the XRD (e) and the TG-DSC of MGPH (f).

cellulose [24]. As for MGPH, the C-O at 1,015 cm^{-1} disappeared and the carboxylic O-H absorption peak at 3,314 cm^{-1} weakened. These changes show that the cellulose began to decompose and the oxygen-containing functional groups began to decrease after pyrolysis [25]. The decrease of methylene -CH_2 at 2,918 cm^{-1} and the out of plane bending vibration of aromatics C-H at 791 and 891 cm^{-1} shows that biochar began demethylation and the degree of aromatization increased [26]. A weak band at 1,281 cm^{-1} was assigned to C-H in plane deformation. The absorption peak at 1,439.05 cm^{-1} is due to C=C vibration in the benzene ring, and the absorption peak at 1,281.68 cm^{-1} is due to the vibration of the phenolic hydroxyl group Ph-OH, both characteristic peaks of PDA [27]. These results verify to a certain extent that the PDA polymer was modified on the surface of GPH [26].

XPS was further used to analyze the chemical composition and electronic structural of MGPH. The general scan spectrum of MGPH shows the presence of stronger N 1s peak compared to that of GPH (Fig. S2). After modification, the N 1s peak of MPGH increased, suggesting the presence of more N elements on the surface of MGPH. This may be attributed to the chemical composition of PDA which was xv coated on the surface of GPH [26].

XRD patterns of the GP, GPH and MGPH are shown in Fig. 1(e). There is a diffraction peak at 2θ=22° in GP; after modification, it was found that the broad peak moved to 23°, a slightly higher 2θ. This might be related to the interaction between grapefruit peel and polydopamine, resulting in the defect formation and lattice distance reduction [28,29]. The sample was amorphous from the peaks observed in the XRD pattern [30]. The peaks around 2θ=20° are characteristic peaks of amorphous carbon, and the diffraction peak intensity of carbon crystals on MGPH was reduced compared to GP because it was re-fixed during hydrothermal activation [31]. These abundant carbons on MGPH acted as π donors, which could release electron-rich π clouds. Electron-deficient fluoroquinolone antibiotics were considered π acceptors, which could interact with MGPH through π-π electron donor-acceptor interactions to facilitate adsorption [32,33].

TG-DSC analysis of MGPH is shown in Fig. 1(f). The figure shows that there is an obvious weight loss peak at 150 °C, which is equivalent to 3% of the total weight, representing the removal of low boiling point volatile organic compounds. Rapid weight loss in the range of 300-450 °C might be related to the decomposition of residual lignin and other inorganic salts [34], which account for 42% of the total weight. The peak at 370 °C (DSC curve) supports the decomposition of polydopamine [35]. The sustained weight loss of MGPH above 450 °C might be related to the reaction between coke, carbon skeleton and volatile gases released from the previous stage [36].

2. Effect of Solution pH on Adsorption

The adsorption capacity of MGPH for ENO and OFLX at different initial solution pH (2-10) is shown in Fig. 2(a) and Fig. 2(b), respectively. The adsorption capacity of ENO by MGPH increased with the increasing of pH (Fig. 2(a)). It is well known that ENO (pK_a=5.31/8.68) and OFLX (pK_a=6.01/8.25) are amphoteric molecules (Fig. S4), and both adsorbates were in the form of cationic species (ENO^+ and $OFLX^+$) when the solution pH<pK_{a1}, neutral species ($ENO^{\pm}$ and $OFLX^{\pm}$) at solution pH lay between pK_{a1} and pK_{a2}, and anionic species (ENO^- and $OFLX^-$) at solution pH> pK_{a2}. ENO possesses a carboxylic acid group (pK_{a1}=5.31) and an amine group in the piperazine ring (pK_{a2}=8.68) [37]. And the acid and basic groups make the solubility and lipophilicity of ENO dependent on pH (Fig. S4(a)). This might be due to the electrostatic attraction between MGPH and ENO because the MGPH surface was negatively charged and ENO was mainly in the form of cationic species [15]. While, ENO gradually tended to deprotonate

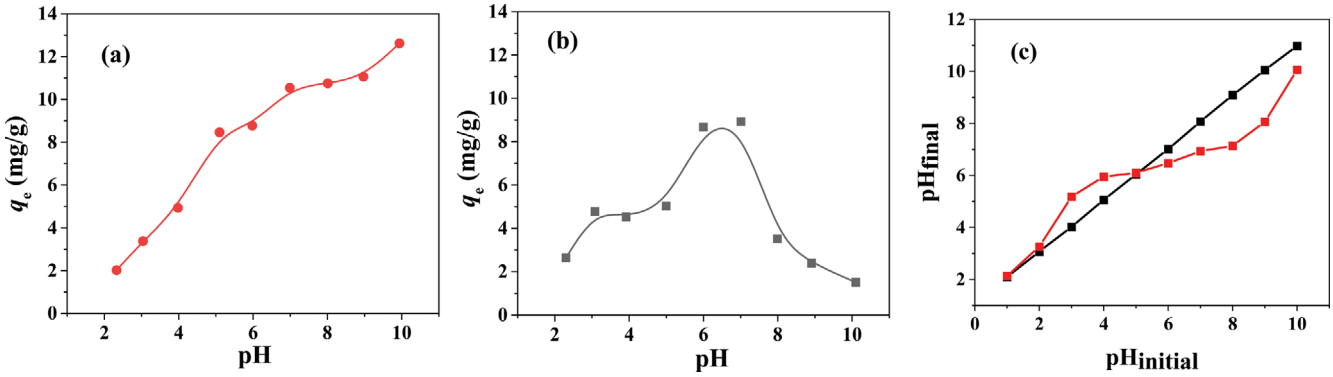

Fig. 2. The effect of pH on the adsorption of ENO (a) and OFLX (b) and the variation of point of zero charge with equilibrium pH of MGPH suspensions (c).

Table 2. Isotherm constants for ENO and OFLX adsorption onto MGPH at different temperatures

Isotherm constants	Temperature/(K)					
	293	303	313	293	303	313
	ENO			OFLX		
Langmuir						
q_m/(mg g^{-1})	36.9744±5.8772	37.6087±2.9041	39.7830±4.2082	81.8088±80.6676	25.3324±7.4319	27.2177±8.7285
K_L/(L mg^{-1})	0.0148±0.0042	0.0165±0.0024	0.0172±0.0034	0.0019±0.0021	0.0103±0.0048	0.0108±0.0055
R^2	0.962	0.989	0.979	0.979	0.953	0.940
Freundlich						
K_F	1.1660±0.3294	1.3955±0.2558	1.5296±0.3443	0.1698±0.0612	0.4664±0.2106	0.5469±0.2599
1/n	0.6573±0.0701	0.6322±0.0458	0.6289±0.0565	0.9528±0.0866	0.7366±0.1105	0.7235±0.1168
R^2	0.948	0.975	0.962	0.976	0.931	0.919
Redlich-Peterson						
A	0.5141±0.1823	0.5819±0.1064	0.6049±0.1262	0.1487±0.0063	0.1981±0.0136	0.2274±0.0249
B	0.0076±0.0302	0.0086±0.0162	0.0045±0.0118	3.71E-20±3.7E-18	1.78E-09±1.9E-08	4.64E-08±5.8E-07
g	1.1278±0.7661	1.1237±0.3605	1.2616±0.5242	9.8080±21.4942	4.4541±2.4486	3.7361±2.7746
R^2	0.962	0.989	0.980	0.993	0.984	0.966
Dubinin-Radushkevich (D-R)						
q_m/(mg g^{-1})	18.3131±0.9891	19.6236±1.0666	21.0944±1.1694	11.1653±0.7417	11.3221±0.5516	12.4866±0.8708
E_a/(kJ mol^{-1})	104.8097±11.6097	108.9688±12.1696	112.9307±12.6659	60.9477±5.6755	81.8019±6.6161	84.4998±9.7854
R^2	0.908	0.903	0.902	0.950	0.960	0.919

and converted to neutral or anionic species with pH increasing, herein the electrostatic repulsion was enhanced [38]. The OFLX has two pK_a values (pK_{a1}=5.45 and pK_{a2}=6.2) [39] indicating that when pH<5.45, 5.45<pH<6.2, pH>6.2, OFLX mainly existed as $OFLX^+$, $OFLX^{\pm}$, and $OFLX^-$, respectively (Fig. S4(b)). The sorption of OFLX on pH-dependence shows a bell-shaped curve (Fig. 2(b)). The results are consistent with previous findings of CIP sorption on Fe oxides [40]. The zero potential charge (pH_{zpc}) of MGPH was 5 (Fig. 2(c)). When the solution pH<pH_{zpc}, its surface was electropositive, and when pH>pH_{zpc}, its surface was electronegative. Therefore, at pH<5.45 and pH>6.2, the decreased adsorption capacity might be due to the significant electrostatic repulsion between OFLX and MGPH. Furthermore, the results show that in addition to electrostatic interactions, chemical interactions were also an influencing factor in the adsorption process [41].

3. Adsorption Equilibrium Isotherms

The adsorption isotherm results fitted by the isotherm models mentioned above at three different temperatures are shown in Fig. S5 and Table 2. As shown in Table 2, the Langmuir isotherm and Redlich-Peterson model show a good fit to adsorption data of ENO and OFLX (R^2>0.94). Hence, the adsorption of ENO and OFLX is a monolayer adsorption on a uniform surface [42]. The maximum adsorption capacity of ENO and OFLX according to Langmuir model was 36.97 mg g^{-1} and 81.81 mg g^{-1}, respectively. Comparison of different adsorbents for ENO and OFLX adsorption is summarized in Table S2. Although the values of adsorption capacity were obtained at different experimental conditions, the results show that MGPH can be considered as a promising adsorbent for ENO and OFLX removal from aqueous solutions. In addition, the Freundlich constant (1/n) is often used to determine whether the ad-

Table 3. Kinetic parameters of ENO and OFLX adsorption onto MGPH

Kinetic patameters	C_0/(mg/L)					
	30	50	80	30	50	80
	ENO			OFLX		
Pseudo-first-order equation						
k_1/(min^{-1})	0.0474±0.0034	0.0783±0.0068	0.0895±0.0120	0.0481±0.0062	0.1357±0.0489	0.0603±0.0128
q_e(exp)/(mg g^{-1})	5.2855	7.8401	11.1526	4.2462	6.6583	8.1407
q_e(cal)/(mg g^{-1})	5.2261±0.1281	7.5536±0.1763	10.9240±0.4379	4.2302±0.1741	5.7646±0.5564	7.6663±0.3343
R^2	0.989	0.984	0.959	0.977	0.578	0.976
Pseudo-second-order equation						
k_2/(g mg^{-1} min^{-1})	0.0087±0.0016	0.0117±0.0008	0.0106±0.0015	0.0100±0.0026	0.0310±0.0122	0.0077±0.0019
q_e(cal)/(mg g^{-1})	6.0486±0.2732	8.3397±0.1070	11.6859±0.3250	5.0967±0.3192	6.3848±0.4820	8.9688±0.4170
R^2	0.979	0.997	0.985	0.975	0.814	0.988
Elovich equation						
a	0.5007±0.1607	1.7180±0.4631	3.9106±1.1155	0.3745±0.1158	5.1067±1.5561	0.9207±0.3089
b	0.7257±0.1069	0.6259±0.0553	0.4969±0.0413	0.7864±0.1264	0.9678±0.0774	0.4742±0.0668
R^2	0.946	0.974	0.976	0.958	0.969	0.977
Double-constant rate equation						
a	0.9386±0.2603	2.0022±0.3665	3.2902±0.4837	0.6799±0.2011	2.3647±0.1008	1.3994±0.4418
K_s	0.3561±0.0625	0.2824±0.0414	0.2499±0.0334	0.4051±0.0705	0.2211±0.0113	0.3813±0.0730
R^2	0.877	0.923	0.939	0.906	0.986	0.937
Intraparticle diffusion model						
k_{t1}/(mg g^{-1} $min^{-0.5}$)	0.9067±0.0717	1.0637±0.1576	1.8169±0.7143	0.8074±0.0486	0.5710±0.0926	0.7275±1.1299
C_1/(mg g^{-1})	–0.8790±0.2869	0.2876±0.5827	0.3462±1.7003	0.1619±0.1667	2.0631±0.2986	0.4335±0.3767
R	0.991	0.959	0.931	0.996	0.963	0.755
k_{t2}/(mg g^{-1} $min^{-0.5}$)	0.1811±0.0478	0.2512±0.0715	0.4534±0.0690	4.2462	0.3460±0.0927	0.3544±0.0850
C_2/(mg g^{-1})	3.0405±0.4679	4.8311±0.7008	5.8416±0.5917	0	3.0832±0.8291	4.2785±0.7364
R	0.910	0.897	0.947	-	0.966	0.947

sorption process was favorable. The value of 1/n is less than 1, indicating that the adsorption process was favorable [43].

4. Adsorption Kinetics

As shown in Fig. S6, the adsorption of ENO and OFLX increased rapidly with contact time during the first 30 min, then became slow and then remained stable. It can be seen from the results that the adsorption process was divided into fast adsorption and slow adsorption. This fast adsorption might be due to the large number of unoccupied active sites. After a period of time, the active sites of MGPH were occupied and the adsorption saturation was reached [44]. To better understand the adsorption kinetics of ENO and OFLX by MGPH, four different kinetic models were adopted. Fitting results are displayed in Fig. S3 and Table 3. Obviously, the criterion of the correlation coefficient (R^2) is consistent with the closeness between the experimental data and adsorption capacities calculated by the models, indicating the relatively great correlation of Elovich and pseudo-second-order models. The adaptability of Elovich and pseudo-second-order models reveals that the adsorption process of ENO and OFLX on MGPH is dominated by chemical adsorption [45,46]. Considering the porous structure of MGPH, IPD was used to further determine the diffusion mechanism of ENO and OFLX on MGPH. According to previous studies, if the plot of q_t versus $t^{1/2}$ gives a straight line through the origin, then intra-particle diffusion is considered to be the only rate-controlling step [47]. As shown in Fig. S7, before reaching the adsorption equilibrium, a straight line was given between q_t and $t^{1/2}$, but the line did not pass through the origin, suggesting that intra-particle diffusion dominated the adsorption process, but was not the only rate control step.

5. Adsorption Thermodynamics

Thermodynamically relevant parameters are shown in Table 4. The results show that ΔG was negative during the adsorption of ENO and OFLX by MGPH in this study, indicating that the adsorption was spontaneous. Furthermore, ΔG decreased with increasing temperature, which indicates that increasing temperature favors adsorption [48]. The ΔH was positive, indicating that the adsorption process was endothermic [47]. The result was the same as that of Gibbs free energy. ΔS was also positive, indicating that adsorption was an entropy-increasing process.

6. Adsorption Mechanisms

MGPH had greater adsorption potential than GPH (Fig. S8), probably because it had more functional groups. Functional groups containing C, H and N played a key role during the controlled adsorption process. In particular, functional groups containing H and O/F played an important role in the formation of complexes with organic pollutants, and the formation of hydrogen bonds and π-π

Table 4. Thermodynamic parameters for ENO and OFLX adsorption onto MGPH

Adsorbents	ΔH (kJ mol^{-1})	ΔS (J mol^{-1} K^{-1})	ΔG (kJ mol^{-1})		
			293 K	303 K	313 K
ENO	31.12	0.13	−8.01	−9.97	−10.70
OFLX	46.36	0.17	−3.66	−5.55	−7.08

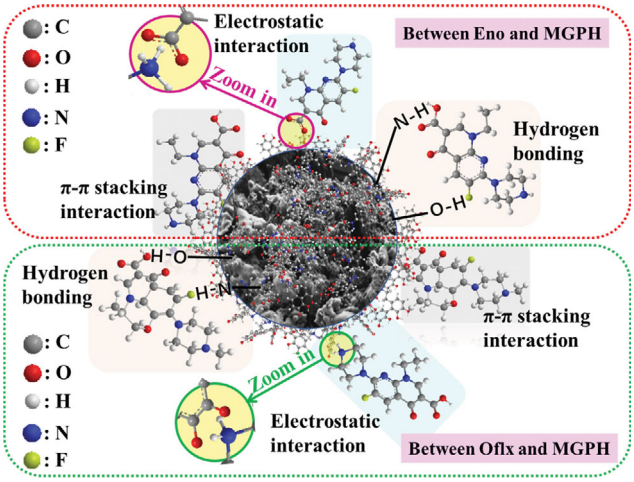

Fig. 3. The proposed adsorption mechanisms of ENO and OFLX on MPGH.

stacking interaction between adsorbents and antibiotics were beneficial for adsorption [16,49]. In addition, the formation of polar covalent bonds between antibiotics and N and O elements in MGPH could have enhanced their removal efficiency [50]. Especially, high aromaticity increased the hydrophobicity of MGPH, thereby enhancing their chemo-attractive affinity for organic pollutants [51]. The proposed adsorption mechanisms of ENO and OFLX on MPGH are shown in Fig. 3.

CONCLUSIONS

MGPH with rich functional groups, excellent porous structure and carbon structure was successfully synthesized by carbonization of dry grapefruit peel by hydrothermal method and surface modification with dopamine. Redlich-Peterson model and Elovich model well described the experimental data, and the results of characterization and thermomechanical analysis showed that the adsorption of both fluoroquinolone antibiotics mainly relied on π-π stacking interaction, hydrogen bond and electrostatic interaction. In conclusion, this study provides a new and potential method for the adsorption removal of ENO, OFLX and other antibiotics. However, in future research, the application of adsorbent materials must be considered and approved to improve the reusability of adsorbents.

ACKNOWLEDGEMENTS

The authors would like to acknowledge the financial support provided by research funds from the financial support of National Natural Science Foundation of China (No. 41807120), the Cultivation Plan for Young Core Teachers in Universities of Henan Province (No. 2021GGJS063), Science and Technology Foundation of Henan Province (No. 212102310026, No. 202102310233) and the Young Backbone Teachers Training Program Foundation of Henan University of Technology.

CONFLICTS OF INTEREST

None.

SUPPORTING INFORMATION

Additional information as noted in the text. This information is available via the Internet at http://www.springer.com/chemistry/journal/11814.

REFERENCES

1. T. B. Nguyen, Q. M. Truong, C. W. Chen, W. H. Chen and C. D. Dong, *Bioresour. Technol.*, **351**, 127043 (2022).
2. M. Stylianou, A. Christou, C. Michael, A. Agapiou, P. Papanastasiou and D. Fatta-Kassinos, *J. Environ. Chem. Eng.*, **9**, 105868 (2021).
3. I. Alacabey, *Molecules*, **27**, 1380 (2022).
4. X. Cao, Z. Meng, E. Song, X. Sun, X. Hu, L. Wenbin, Z. Liu, S. Gao and B. Song, *Chemosphere*, **299**, 134414 (2022).
5. H. Wang, X. Lou, Q. Hu and T. Sun, *J. Mol. Liq.*, **325**, 114967 (2021).
6. E. Marris, *Nature*, **442**, 624 (2006).
7. J. Lehmann, *Nature*, **447**, 143 (2007).
8. J. Chen, J. Ouyang, W. Lai, X. Xing, L. Zhou, Z. Liu, W. Chen and D. Cai, *Sep. Purif. Technol.*, **279**, 119700 (2021).
9. D. Lv, Y. Li and L. Wang, *Int. J. Biol. Macromol.*, **148**, 979 (2020).
10. M. Imran, A. Islam, M. U. Farooq, J. Ye and P. Zhang, *Environ. Sci. Pollut. Res.*, **27**(35), 43493 (2020).
11. Z. Wang, P. Jin, M. Wang, G. Wu, C. Dong and A. Wu, *ACS Appl. Mater. Interfaces*, **8**(48), 32862 (2016).
12. X. Geng, S. Lv, J. Yang, S. Cui and Z. Zhao, *J. Environ. Manage.*, **280**, 111749 (2021).
13. W. Zhang, J. Song, Q. He, H. Wang, W. Lyu, H. Feng, W. Xiong, W. Guo, J. Wu and L. Chen, *J. Hazard. Mater.*, **384**, 121445 (2020).
14. Z. Huang, C. Xiong, M. Zhao, S. Wang, Y. Zhou, L. Dai and L. Zhang, *Adv. Powder Technol.*, **32**(4), 1013 (2021).
15. L. Wu, X. Zhang and Y. Si, *Mater. Chem. Phys.*, **279**, 125767 (2022).
16. M. Ahmad, S. S. Lee, X. Dou, D. Mohan, J. K. Sung, J. E. Yang and Y. S. Ok, *Bioresour. Technol.*, **118**, 536 (2012).
17. M. Ahmad, S. S. Lee, A. U. Rajapaksha, M. Vithanage, M. Zhang, J. S. Cho, S. E. Lee and Y. S. Ok, *Bioresour. Technol.*, **143**, 615 (2013).
18. H. Ao, W. Cao, Y. Hong, J. Wu and L. Wei, *Sci. Total Environ.*, **708**, 135092 (2020).

19. L. Akhtar, M. Ahmad, S. Iqbal, A. A. Abdelhafez and M. T. Mehran, *Environ. Technol. Innovation*, **24**, 101912 (2021).
20. Y. Bulut and H. Aydın, *Desalination*, **194**(1-3), 259 (2006).
21. H. Bai, J. Chen, Z. Wang, L. Wang and E. Lamy, *J. Chem. Eng. Data*, **65**(9), 4443 (2020).
22. H. Yu, L. Gu, L. Chen, H. Wen, D. Zhang and H. Tao, *Bioresour. Technol.*, **316**, 123971 (2020).
23. D. D. Sewu, P. Boakye and S. H. Woo, *Bioresour. Technol.*, **224**, 206 (2017).
24. Y. Liu, H. G. Chae and S. Kumar, *Carbon*, **49**(13), 4487 (2011).
25. M. A. Khan, S. Khan, X. Ding, A. Khan and M. Alam, *Chemosphere*, **193**, 1120 (2018).
26. X. Yu, H. Fan, Y. Liu, Z. Shi and Z. Jin, *Langmuir*, **30**(19), 5497 (2014).
27. H. Xu, J. Sun, H. Wang, Y. Zhang and X. Sun, *Food Chem.*, **365**, 130409 (2021).
28. H. Dong, X. Guo, C. Yang and Z. Ouyang, *Appl. Catal. B: Environ.*, **230**, 65 (2018).
29. S.-Y. Yang, K.-H. Chang, Y.-L. Huang, Y.-F. Lee, H.-W. Tien, S.-M. Li, Y.-H. Lee, C.-H. Liu, C.-C. M. Ma and C.-C. Hu, *Electrochem. Commun.*, **14**(1), 39 (2012).
30. N. Magesh, A. A. Renita, R. Siva, N. Harirajan and A. Santhosh, *Chemosphere*, **290**, 133227 (2022).
31. R. C. Dante, P. Chamorro-Posada, J. Vázquez-Cabo, Ó Rubiños-López, F. M. Sánchez-Árevalo, L. Huerta, P. Martín-Ramos, L. Lartundo-Rojas, C. F. Ávila-Vega, E. D. Rivera-Tapia, C. A. Fajardo-Pruna, Á. J. Ávila-Vega and O. Solorza-Feria, *Carbon*, **121**, 368 (2017).
32. T. Atugoda, C. Gunawardane, M. Ahmad and M. Vithanage, *Chemosphere*, **281**, 130676 (2021).
33. S. H. Ho, Y. D. Chen, R. Li, C. Zhang, Y. Ge, G. Cao, M. Ma, X. Duan, S. Wang and N. Q. Ren, *Water Res.*, **159**, 77 (2019).
34. Y. Xu and B. Chen, *Bioresour. Technol.*, **146**, 485 (2013).
35. N. Rahman, P. Varshney and M. Nasir, *Environ. Nanotechnol., Monit. Manage.*, **15** (2021).
36. L. Emami Taba, M. F. Irfan, W. A. M. Wan Daud and M. H. Chakrabarti, *Renew. Sustain. Energy Rev.*, **16**(8), 5584 (2012).
37. L. Wang, L. Zhang, B. Feng, X. Hua, Y. Li, W. Zhang and Z. Guo, *Sci. Total Environ.*, **823**, 153707 (2022).
38. Y. Ma, T. Lu, L. Yang, L. Wu, P. Li, J. Tang, Y. Chen, F. Gao, S. Cui, X. Qi and Z. Zhang, *Environ. Pollut.*, **298**, 118833 (2022).
39. Y. Wang, Y. Fang, Y. Gu, K. Guo, Z. Guo and C. Tang, *J. Mol. Struct.*, **1255**, 132475 (2022).
40. C. Gu and K. G. Karthikeyan, *Environ. Sci. Technol.*, **39**, 9166 (2005).
41. B. Yao, Z. Luo, S. Du, J. Yang, D. Zhi and Y. Zhou, *Bioresour. Technol.*, **340**, 125698 (2021).
42. S. Xie, L. Wang, Y. Xu, D. Lin, Y. Sun and S. Zheng, *Sci. Total Environ.*, **740**, 140009 (2020).
43. Z. Wang, J. Su, X. Hu, A. Ali and Z. Wu, *J. Hazard. Mater.*, **406**, 124748 (2021).
44. M. E. Mahmoud, A. K. Mohamed and M. A. Salam, *J. Hazard. Mater.*, **408**, 124951 (2021).
45. D. Cheng, H. H. Ngo, W. Guo, S. W. Chang, D. D. Nguyen, X. Zhang, S. Varjani and Y. Liu, *Sci. Total Environ.*, **720**, 137662 (2020).
46. C. Jiang, X. Wang, D. Qin, W. Da, B. Hou, C. Hao and J. Wu, *J. Hazard. Mater.*, **369**, 50 (2019).
47. K. Dong, K. Xu, N. Wei, Y. Fang and Z. Qin, *Chem. Eng. Res. Des.*, **179**, 227 (2022).
48. L. R. Bonetto, J. S. Crespo, R. Guégan, V. I. Esteves and M. Giovanela, *J. Mol. Struct.*, **1224**, 129296 (2021).
49. Y. Ma, T. Lu, L. Yang, L. Wu, P. Li, J. Tang, Y. Chen, F. Gao, S. Cui, X. Qi and Z. Zhang, *Environ. Pollut.*, **298**, 118833 (2022).
50. X. Zhang, Y. Chu, H. Zhang, J. Hu, F. Wu, X. Wu, G. Shen, Y. Yang, B. Wang and X. Wang, *Sci. Total Environ.*, **772**, 145468 (2021).
51. M. Ahmad, A. U. Rajapaksha, J. E. Lim, M. Zhang, N. Bolan, D. Mohan, M. Vithanage, S. S. Lee and Y. S. Ok, *Chemosphere*, **99**, 19 (2014).